Cardiac Phantom Evaluation of Simultaneously Acquired Dual-Isotope Rest Thallium-201/Stress Technetium-99m SPECT Images

Val J. Lowe, Kim L. Greer, Michael W. Hanson, Ronald J. Jaszczak and R. Edward Coleman

Section of Nuclear Medicine, Department of Radiology, Duke University Medical Center, Durham, North Carolina

Simultaneously acquired dual-isotope $^{201}Tl/^{99m}Tc$ SPECT studies were performed using cardiac and thoracic phantoms to evaluate the dual-isotope myocardial perfusion technique. Cardiac phantom images representing infarction, viable myocardium and various levels of ischemia were analyzed. Studies with and without attenuating media were performed, and myocardium-to-defect count ratios and defect sizes from dual-isotope SPECT images were compared to myocardium-to-defect count ratios and defect sizes from single-isotope (^{201}Tl and ^{99m}Tc) SPECT images. Dual-isotope studies also were interpreted qualitatively. Studies with background activity simulating clinical conditions were performed and interpreted qualitatively. Myocardium-to-defect count ratios from both ^{99m}Tc and ^{201}Tl were similar in single-isotope and dual-isotope SPECT images. Thallium-201 and ^{99m}Tc defect sizes were decreased slightly (mean ± s.d., 1.0 ± 1.7 cc for ^{201}Tl and 0.7 ± 1.0 cc for ^{99m}Tc) on dual studies when compared to single studies but were not statistically significant. Dual-isotope image simulations of normal, ischemic and infarcted and viable myocardium were correctly identified by experienced clinicians in 95% of the cases (21/22). Simultaneous dual-isotope $^{201}Tl/^{99m}Tc$ SPECT imaging of cardiac phantoms produced images that had similar myocardium-to-defect count ratios to those produced using single-isotope techniques and were correctly evaluated on qualitative analysis. Changes in defect size related to dual-isotope imaging were minimal and not qualitatively important.

J Nucl Med 1993; 34:1998–2006

Myocardial perfusion imaging using ^{99m}Tc-sestamibi and ^{201}Tl can accurately detect coronary artery disease when used in standard protocols (*1–13*). Studies comparing the two radiopharmaceuticals have revealed similar sensitivities and specificities for the detection of coronary artery disease (*13–21*). Image quality differences between the two radiopharmaceuticals have been reported (*22,23*). Now that both agents are in common clinical use, techniques are being developed to help streamline the studies. Myocardial perfusion imaging by dual-isotope simultaneous acquisition techniques could reduce camera imaging time, the total time that a patient is in an imaging facility and errors induced by image misalignment. Simultaneously acquired dual-isotope rest ^{201}Tl/stress ^{99m}Tc-sestamibi studies are being evaluated for clinical use in some centers (*24*). Separate acquisition dual-isotope techniques have also been evaluated clinically (*25,26*). For simultaneous acquisition, ^{201}Tl is administered prior to exercise and ^{99m}Tc-sestamibi is administered at peak exercise. Imaging is performed after exercise with one simultaneous acquisition using the ^{201}Tl (rest images) and ^{99m}Tc (stress images) photon energy windows. A potential problem with this technique is the ^{99m}Tc downscatter into the ^{201}Tl window which could result in the partial loss of rest image defects. Also, size differences between ^{99m}Tc and ^{201}Tl representations of the same defect have been reported in clinical studies (*17*). An understanding of these defect size differences would be crucial to evaluating the dual-isotope technique.

In this study, we evaluate the differences between defect sizes and myocardium-to-defect count ratios in ^{99m}Tc and ^{201}Tl single- and dual-isotope cardiac phantom studies, evaluate dual-isotope myocardial defect recognition in cardiac phantoms and provide examples of dual-isotope cardiac phantom SPECT images with attenuating media and background activity.

METHODS

Phantom Preparation

Two thoracic phantoms (Data Spectrum Corp., Hillsborough, NC) containing a cardiac phantom were used. Phantom A was an elliptical thoracic phantom (31 cm by 22 cm) with a volume of 10.2 liters, which was filled with water during scans obtained for evaluation of attenuation. Phantom B (Fig. 1) had a volume of 6420 ml with lungs in place and had a posterior solid Teflon® column to simulate the thoracic spine (3.8 cm in diameter). The right and left lungs contained 1180 ml and 885 ml and had styrofoam beads within them which displaced 800 ml and 615 ml respectively. Water containing a uniform concentration of radionuclide was added to the lungs and thoracic cavity for scans using phantom B.

The cardiac phantom had a myocardial volume of 120 ml that surrounded a central cavity. Three myocardial defects were used. A small defect had a total displacement volume of 4.9 ml and

Received Nov. 3, 1992; revision accepted Jun. 20, 1993.

For correspondence or reprints contact: Val J. Lowe, MD, Section of Nuclear Medicine, Box 3949, Department of Radiology, Duke University Medical Center, Durham, NC 27710.

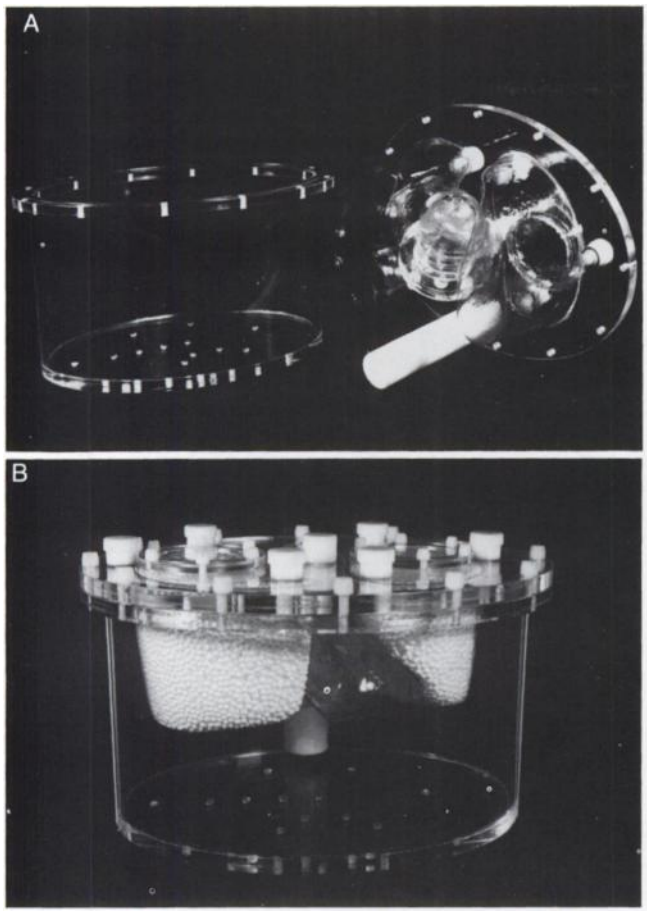

FIGURE 1. Thorax phantom B (A) disassembled and (B) assembled with lung beads in place.

contained 2.6 ml of fluid. A medium defect had a total displacement volume of 9.5 ml and contained 5.8 ml of fluid. A large defect had a total displacement volume of 19.2 ml and contained 11.8 ml of fluid. The defects were placed about 2.5 cm from the apex of the phantom in similar positions.

Radioactivity concentrations were chosen to mimic the known myocardial uptake of ^{201}Tl and ^{99m}Tc-sestamibi (3% and 1.1% of the injected dose respectively) (*5,27*). Injected doses of 4.0 mCi (148 MBq) of ^{201}Tl and 17.0 mCi (629 MBq) of ^{99m}Tc-sestamibi were used as a basis for myocardial dose calculation. To minimize acquisition time, activity concentrations threefold higher than known myocardial uptake were used in phantom A studies. Water was used to fill the myocardial defect if no activity was desired. In preparing phantom B, lung and background activity was prepared to mimic the roughly 2:1 myocardium-to-lung and 2:1 myocardium-to-background count ratios that are generally reported (*5,9,22,27*). For accurate activity counting with a multichannel analyzer, 1-2-ml solution samples were removed from the structures in phantom B.

Thirty-six different phantom studies were performed and the decay-corrected activity concentrations are shown in Table 1. The first 34 acquisitions were performed with and without attenuating media (two acquisitions were performed with attenuating media only) using phantom A and included the following radioactivity distributions (the clinical situations mimicked are shown in parentheses):

1. Technetium-99m filled myocardium with water in the defect (infarct-single agent).
2. Thallium-201 filled myocardium with water in the defect (infarct-single agent).
3. Technetium-99m and ^{201}Tl filled myocardium with no defect (normal).
4. Thallium-201 and ^{99m}Tc filled myocardium with water in the defect (infarct-dual agent).
5. Technetium-99m and ^{201}Tl filled myocardium with ^{201}Tl only in the defect (severe ischemia).
6. Technetium-99m and ^{201}Tl filled myocardium with ^{201}Tl and one-third of the myocardial ^{99m}Tc activity in the defect (moderate ischemia).
7. Technetium-99m and ^{201}Tl filled myocardium with ^{201}Tl and two-thirds of the myocardial ^{99m}Tc activity in the defect (minimal ischemia).
8. Technetium-99m and ^{201}Tl filled myocardium with ^{201}Tl in the defect at one-half of the myocardial ^{201}Tl activity (viable myocardium).

The last two phantom acquisitions were performed using phantom B. One of these studies used ^{99m}Tc and ^{201}Tl filled myocardium with water in the defect (infarct) and the other used ^{99m}Tc and ^{201}Tl filled myocardium with ^{201}Tl and 66% of the myocardial ^{99m}Tc activity in the defect (minimal ischemia).

Imaging Techniques

The data were acquired on a Trionix Triad 88 (Trionix Research Laboratories, Inc., Twinsburg, OH) triple-head SPECT scanner. The scans were configured to approximate the conditions of patient scans. Simultaneous, dual-energy window settings were used for each camera. The first energy window was 15% (FWHM) wide (129–151 keV) and set symmetrically over the 140-keV peak of ^{99m}Tc. The second window was 30% (FWHM) wide (59–81 keV) and set asymmetrically over the ^{201}Tl x-ray prominence centered approximately at 70 keV. When dual-energy window scans were acquired, the data from each window were binned into separate frames for each projection angle. As with the typical patient scans, the gantry rotation was for 120 degrees, thus providing a full 360 degrees of data because all three heads collected data. Gantry rotation was of the step-and-shoot method, pausing for images each 3 degrees of rotation. Each head collected 40 views per energy window during the 120 degrees of rotation. The images were acquired into 128 × 128, 2 byte, unsigned short integer frames. The zoom factor was 1.0 and produced pixels with dimensions of 3.56 × 3.56 mm within the projection data. The data for each energy window for each stop were kept separate to allow for reconstruction of the ^{99m}Tc and the ^{201}Tl acquisitions separately. The phantom was scanned with a noncircular gantry orbit, which had a minor axis (antero-posterior direction) radius of approximately 14.0–14.5 cm and a major axis radius of approximately 16.0–16.5 cm. A LEUR (low energy, ultra-high resolution) collimator was used. The total scan time was varied to produce projection sets with approximately the same total counts as would be encountered with patient studies, based on the amounts of radioactivity placed in the various phantom chambers. Generally, approximately 13 sec were used per stop for 40 stops for a total scan time of 520 sec.

The phantom was centered on the camera's axis of rotation. The phantom has a mounting bracket which allows for precise relocation from one scan set to the next. Positioning was facilitated with the use of a ceiling-mounted laser. The phantom was positioned in the same location throughout all the scan sets.

TABLE 1
Activity Concentrations and Count Ratios

Thorax A Studies	Regions	Activity ^{99m}Tc*	Activity ^{201}Tl*	Count ratio ^{99m}Tc*	Count ratio ^{201}Tl*
Single agent*					
Defects					
Small no attn	myoc/defect	5.5/0	5.0/0	2.94	2.73
attn	myoc/defect	5.3/0	5.0/0	2.93	2.62
Medium no attn	myoc/defect	5.2/0	5.0/0	3.33	3.21
attn	myoc/defect	5.3/0	4.9/0	3.12	2.80
Large no attn	myoc/defect	5.0/0	5.0/0	3.88	3.71
attn	myoc/defect	4.9/0	4.9/0	3.36	3.08
Dual agents					
Normal attn	myoc/defect	5.7/5.7	4.8/4.8	1.05	1.01
Defects (infarct)					
Small no attn	myoc/defect	5.6/0	5.3/0	2.84	2.60
attn	myoc/defect	5.4/0	5.2/0	2.96	2.53
Medium no attn	myoc/defect	5.2/0	5.2/0	3.24	2.51
attn	myoc/defect	5.0/0	4.9/0	2.82	2.96
Large no attn	myoc/defect	5.1/0	5.2/0	3.26	2.82
attn	myoc/defect	4.9/0	5.2/0	3.98	3.63
Defects (viable myoc)					
medium no attn	myoc/defect	5.3/0	4.4/2.3	3.15	1.79
attn	myoc/defect	5.6/0	4.4/2.3	3.02	2.51
Defects (sev isch)					
Medium attn	myoc/defect	4.6/0	4.8/4.8	3.01	1.16
Defects (mod isch)					
Small no attn	myoc/defect	5.2/1.6	4.6/5.2	2.38	1.39
attn	myoc/defect	5.2/1.6	4.5/5.2	2.22	1.85
Medium no attn	myoc/defect	5.1/1.7	4.4/4.3	2.43	1.33
attn	myoc/defect	4.9/1.6	4.4/4.3	2.65	2.01
Large no attn	myoc/defect	5.2/1.6	4.5/5.2	2.53	1.34
attn	myoc/defect	5.1/1.5	4.3/5.2	2.47	1.72
Defects (min isch)					
Small no attn	myoc/defect	5.1/2.7	4.2/5.1	2.06	1.43
attn	myoc/defect	5.1/2.6	4.1/5.1	2.22	1.91
Medium no attn	myoc/defect	4.6/3.1	4.4/4.6	NA†	NA†
attn	myoc/defect	4.7/3.2	4.4/4.6	2.18	1.89
Large no attn	myoc/defect	5.1/2.5	3.9/5.1	2.16	1.30
attn	myoc/defect	5.1/2.4	3.8/5.1	2.23	1.77
Thorax B studies					
Medium defect					
Infarct	myoc/defect	1.8/0	1.7/0	3.15	1.77
	myoc/chest	0.47	0.26	2.57	2.04
	myoc/R lung	0.53	0.21	1.85	2.22
Medium defect					
Severe ischemia	myoc/defect	1.6/1.0	1.7/1.8	1.41	0.87
	myoc/chest	0.40	0.25	2.42	1.93
	myoc/R lung	0.46	0.21	1.77	2.28

*Data are for separate acquisitions for each isotope in the single studies.
†No defects were found by the size determination program.

Camera uniformity correction is automatically performed in real time during the acquisition. Uniformity was verified each day by the acquisition of a sheet source image for each gamma camera. The center of rotation correction (COR) is optionally performed in real time during acquisition. We chose to use this option during acquisitions. A unique set of COR values for each camera was calculated on each day prior to the phantom scans. The COR offset compensations and uniformity compensations were loaded into the acquisition hardware prior to the scans.

Image Reconstruction

The images were reconstructed into sub-matrices of 32 × 32, 64 × 64 or 128 × 128, depending on the field of view required to image particular structures. However, the same pixel size was

always used (3.56 mm per pixel side). When the lungs were included, this larger field of view made reconstruction into a 128 × 128 array necessary. All image sets were reconstructed with a generalized Hann filter with a cutoff set to 1.0 cycles per cm. The Nyquist frequency used for the selected acquisition parameters was 1.40 cycles per cm. To lower noise without having to choose a smoother filter cutoff frequency, axial smoothing was used with weights of 1-2-1 for smoothing over three slices and was done to take advantage of counts acquired in adjacent slices, which are sampled at less than the expected system resolution. The 128 × 128 matrix size used for the acquisitions corresponds to approximately 3.56 mm per pixel size and provided some additional smoothing without excessively reducing resolution. When oblique angle images (long-axis and short-axis) were produced for a given scan, one of the energy window's transverse images was manually rotated in the transverse and sagittal planes to produce the amount of rotation necessary. Manual rotation is performed by interactively producing the rotation based on a graphic representation of the image and mouse-driven cursor (across which is spun and centered using the mouse). The computer reports the number of degrees for each orientation that the image set is rotated. These numbers were recorded and used for the second energy window rotations by specifying the specific number of degrees to rotate the second energy window, producing exactly the same rotations for both the ^{99m}Tc and the ^{201}Tl images.

Data Analysis

Defect sizes were determined using the Trionix bull's-eye program, which produces a polar and rectangular histogram plot. These calculations were not normalized. The plots were calculated from the individual short-axis image set. The resulting rectangular plot image was saved and read into a locally written program that performed size calculations. The size calculations were based on input coordinates individually selected to encompass an area minimally larger than the observed defects on each separate acquisition. The program searched through the same slice levels (as specified in the input coordinates) for an area outside the defect boundary of the same size to determine the mean counts/pixel, which was defined as the normal myocardial activity. The program then searched the input coordinate region to locate any pixel with less than 50% of the counts in the normal area. These pixels were defined as the defect. Average counts/pixel in the defect were then calculated. For the dual-energy studies, when thallium was in the defect and no thallium defect was found by the program, average ^{201}Tl counts were calculated using the defect size determined in the ^{99m}Tc window.

Since the original image slice thickness was known (0.356 mm per slice in any orientation), the program could relate the rectangular projection's dimensions to original pixel dimensions. The depth of the pixel rows was not directly known but was assumed to be the difference between the outer and inner circumference of the cardiac phantom. This assumption is likely valid because the defect sizes were determined in phantoms that had no background activity. This depth dimension was determined visually by the operator. Knowing defect depth and x and y dimensions as determined by the program on the rectangular region in terms of pixels, the volume of the defects could be calculated because pixel size was known. This conversion would not be valid for defects near the apex and therefore the defects were placed 2.5 cm from the apex.

To test the variability of the size determination method, two single-isotope phantoms (one with ^{99m}Tc and one with ^{201}Tl using the medium sized defect) were imaged three times serially, without alteration between acquisitions, and defect sizes were calculated. Myocardium-to-defect count ratios between single-isotope and dual-isotope studies were compared. Ratios were corrected for slight differences in activity concentrations that had occurred. Defect sizes for ^{99m}Tc and ^{201}Tl acquisitions, between dual- and single-isotope acquisitions for each particular isotope, and between studies with and without attenuating media were compared.

For the two studies performed with phantom B, myocardium-to-lung and myocardium-to-thorax count ratios were also obtained. Regions of interest in lungs and background were drawn as multiple polygon regions and were averaged to obtain counts/pixel.

For qualitative analysis, all dual acquisition images were formatted in our institution's standard exercise/rest displays with vertical long-axis, horizontal long-axis and short-axis views. The images were then presented to two experienced observers (REC, MH) who evaluated the images for the presence of either infarct or ischemia.

RESULTS

A summary of the phantom count ratio data is provided in Table 1. A reduction of 10% (mean ± s.d., 0.3 ± 0.5) in the myocardium-to-defect count ratios for ^{201}Tl was seen in the dual-isotope studies (^{99m}Tc and ^{201}Tl; infarct) from the values seen in the single studies. The count ratios for ^{99m}Tc in the dual-isotope studies showed a 2.0% (0.07 ± 0.4) reduction from the values obtained in the single-isotope studies. The three serial imaging studies to test defect size measurement variability demonstrated that the defect size measurement method had a standard deviation of ±0.1 cc in ^{99m}Tc (mean of 6.9 cc) and ±0.5 cc in ^{201}Tl (mean of 7.25 cc) studies. Defect sizes (Table 2) measured on the ^{99m}Tc studies were larger than those on the ^{201}Tl studies in dual-isotope (0.5 ± 1.5 cc) studies representing infarct but were minimally smaller than ^{201}Tl studies on the single-isotope studies (0.03 ± 1.0 cc) (Fig. 2). Defect sizes were smaller on dual studies than on single studies when measured on the ^{201}Tl studies (1.0 ± 1.7 cc) and ^{99m}Tc studies (0.7 ± 1.0 cc) (Fig. 3). Attenuating media reduced ^{99m}Tc defect sizes in single-isotope studies (0.3 ± 2.0 cc) but increased defect sizes in dual-isotope studies (0.7 ± 2.0 cc). Attenuating media reduced the defect sizes measured on the ^{201}Tl studies for both dual- (1.3 ± 3.1 cc) and single- (1.0 ± 0.5 cc) isotope studies (Fig. 4). Confidence intervals (95%) for the differences in defect sizes between dual studies and single studies (1.0 ± 1.7 cc for ^{201}Tl and 0.7 ± 1.0 cc for ^{99m}Tc) were ±1.8 cc for ^{201}Tl and ±1.0 cc for ^{99m}Tc. The size differences were therefore not significant. Other noted size differences were similar in magnitude to the variability of the defect size measuring method.

The sizes of defects in the moderate and minimal ischemia studies were substantially reduced (2.5 ± 1.1 cc for moderate ischemia and 4.4 ± 3.4 cc for minimal ischemia) from the sizes in the dual-isotope infarct studies (Fig. 5).

Interpretation of the dual-isotope images (Figs. 6, 7) using phantom A was uniformly correct in 19 of 20 studies. The study not correctly identified was in the minimal isch-

TABLE 2
Defect Size Comparison

Thorax A Studies	Defect size (cc) ^{99m}Tc	Defect size (cc) ^{201}Tl
Single agent defects		
Small no attn	3.1	3.7
attn	4.8	3.8
Medium no attn	7.7	7.1
attn	7.0	7.2
Large no attn	18.0	17.0
attn	14.0	15.4
Dual agents defects (infarct)		
Small no attn	4.3	3.0
attn	4.9	4.2
Medium no attn	6.6	5.7
attn	7.8	9.8
Large no attn	17.2	15.5
attn	14.3	13.3
Defects (viable myoc) medium no attn	5.2	1.4
attn	7.1	4.4
Defects (sev isch)		
Medium attn	4.9	0
Defects (mod isch)		
Small no attn	2.7	0
attn	3.6	0.9
Medium no attn	3.6	0
attn	4.9	0.5
Large no attn	12.9	0
attn	9.3	0
Defects (min isch)		
Small no attn	0.3	0
attn	1.9	0
Medium no attn	0	0
attn	1.8	0.1
Large no attn	3.1	0
attn	3.9	0

emia category (medium defect), with attenuating media present and the interpreters disagreeing on the presence of ischemia. Images from phantom B were correctly interpreted (2/2), but readers commented that the images had less contrast than the studies in phantom A (Fig. 8).

DISCUSSION

Myocardial perfusion imaging studies using either ^{99m}Tc-sestamibi or ^{201}Tl-chloride are performed clinically and their accuracy in evaluating coronary artery disease has been well documented (*1–13*). Recently there has been interest in performing simultaneously acquired dual-isotope rest ^{201}Tl/stress ^{99m}Tc-sestamibi studies to shorten acquisition time and patient study time. Dual-isotope imaging in one scan would reduce the potential for errors induced by image misalignment and decrease patient discomfort from longer procedures. Clinical dual-isotope studies are being performed in some centers and have shown promise (*24*). The results of this cardiac phantom evaluation provide support for clinical performance of dual-isotope studies and describe some of the potential benefits and limitations of the procedure.

No direct extrapolation can be made from the results of this phantom study to clinical situations for several reasons. The cardiac phantom was stationary, whereas the lungs and heart are moving in the clinical situation. The small amount of dead space created by the wall material of the defect in the cardiac phantom could overestimate defect contrast and cause studies representing ischemia to appear to have partial infarction. However, to attempt to represent the clinical situation as closely as possible, we prepared both infarct and ischemia models in phantoms that had attenuating media and background activity in the thorax and lungs (phantom B). The cardiac images acquired with attenuating media and background activity were noisier, had less contrast and had more artifacts than

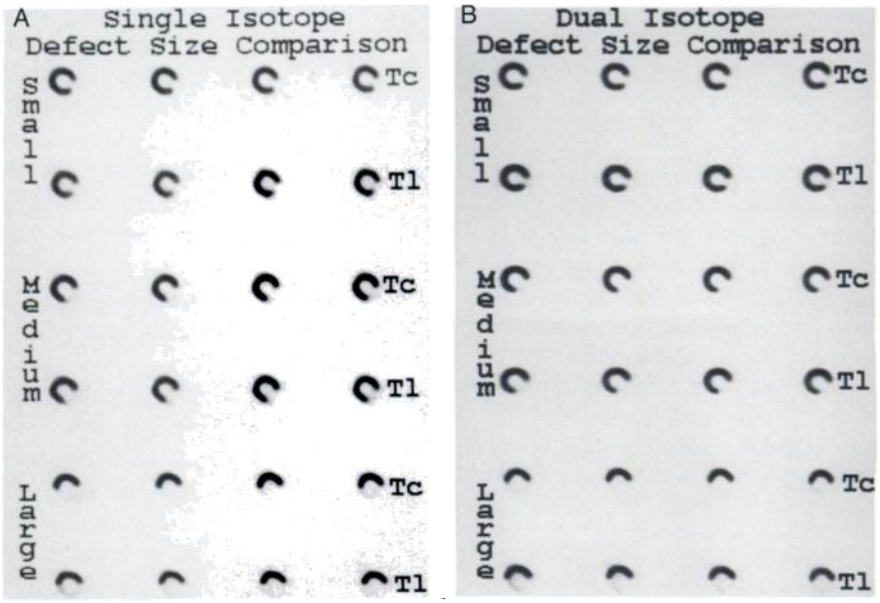

FIGURE 2. Isotope defect size comparisons between single- (A) and dual- (B) isotope studies.

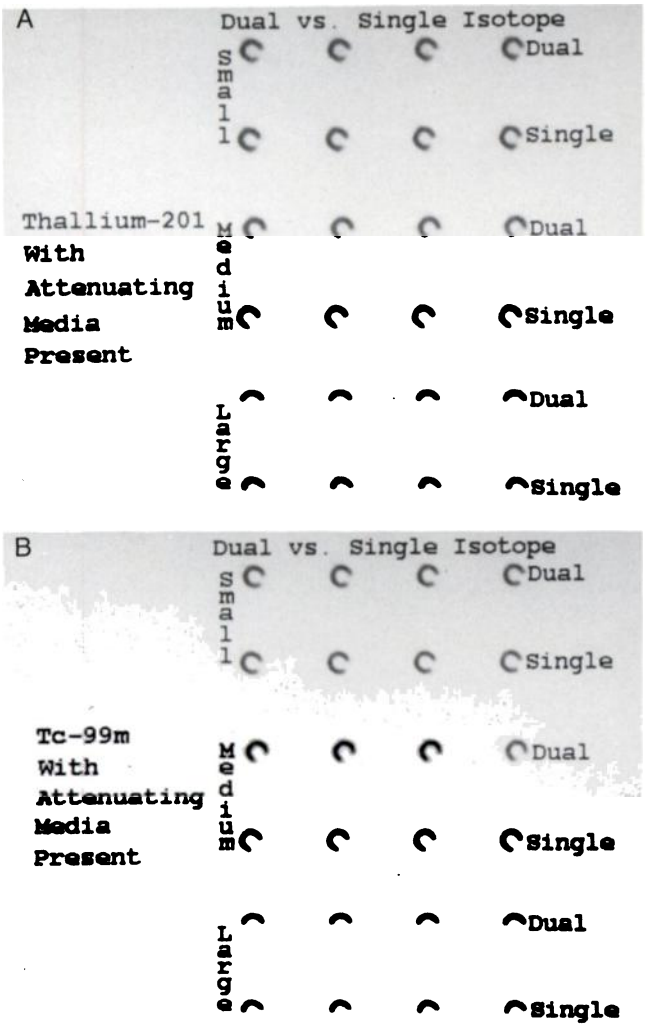

FIGURE 3. Defect size comparison between dual- and single-isotope study for ^{201}Tl (A) and ^{99m}Tc (B). All had attenuating media present.

the images acquired without background activity. An example of an artifact is the loss of counts in the inferior wall of the thallium images (Fig. 8) when no defect was present. This effect has been reported when ^{201}Tl and ^{99m}Tc have been compared in clinical studies (*28*). Defect margins (inferior regions) were also less distinct in the ^{201}Tl images when attenuating media was present (Fig. 4, rows C and D). Increased thickness of attenuating media (from the inferior wall to the thoracic phantom's outer surface) likely alters ^{201}Tl images more than ^{99m}Tc images because of the different photon energies. We note that our results are appropriate only for the specific source configurations, collimation, acquisition protocols and reconstruction procedures that were used. For example, a lower resolution collimator or a different reconstruction filter possibly could alter the magnitude of the effects we observed. It is for these reasons that we selected collimators and reconstruction parameters that were the same as the ones we use with the triple-camera system for routine clinical studies.

Myocardial-to-defect count ratios were compared to evaluate the changes that may occur between single and dual-acquisition studies. A 2.0% decrease in the ^{99m}Tc myocardium-to-defect count ratio was seen in the dual-isotope studies (phantom A: infarct) when compared to the single-isotope study. Thallium-201 emits a 135-keV gamma ray with 2% abundance, which would be included in the ^{99m}Tc window. Our methods were not sensitive enough to evaluate the significance of such small changes, but it is reasonable to assume that any contribution from this photon to the total ^{99m}Tc counts should increase myocardial counts and thereby raise the myocardium-to-defect count ratio in infarcts. Studies done with attenuating media showed a 5% increase in the ^{99m}Tc myocardium-to-defect count ratio when evaluated separately. Activity in the defect may have been more severely reduced when attenuating media were present because the defects were in the inferior and lateral positions and were therefore farther from the thoracic surface than were the areas sampled as normal myocardium.

The accurate differentiation of ischemic myocardium from normal myocardium by the dual-isotope technique should not be hampered by the dual-isotope acquisition technique. In single-day clinical ^{99m}Tc-sestamibi studies, rest activity is present when stress images are being evaluated and does not appear to hamper accurate interpretation of ischemia (*9,11*). In our study, we did not prepare a correlate for this situation, but the interpretation of simultaneously acquired dual-isotope studies for the identification of ischemia would not likely be altered by a 5% increase in the ^{99m}Tc window (stress) counts. Also, any addition to ^{99m}Tc counts from the 135-keV ^{201}Tl photon would occur equally in the myocardium and defect, because ^{201}Tl would be present in both and should have no effect on the myocardium-to-defect ratio.

The potential problem in dual-isotope imaging of ^{99m}Tc downscatter into the ^{201}Tl window causing apparent filling in of resting defects (and areas of infarct to be interpreted as ischemia) has been evaluated clinically and appears to produce only a small underestimation of resting defects (*24*). In our study, the ^{201}Tl myocardium-to-defect count ratio was reduced 10% in the dual-isotope studies (phantom A: infarct) when compared to the single-isotope studies, and this reduction was presumably due to ^{99m}Tc downscatter into the ^{201}Tl window. Nevertheless, defects could

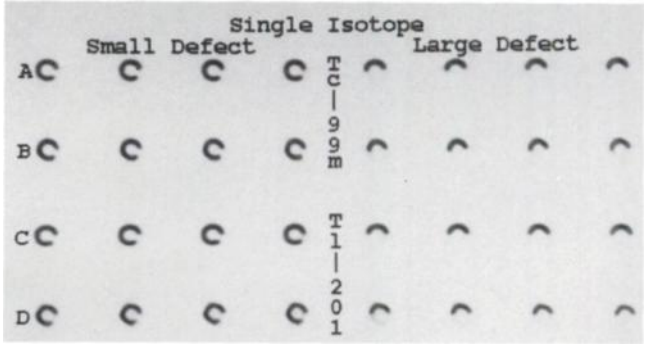

FIGURE 4. Comparison of defect sizes between studies with (rows B and D) and without attenuating media (rows A and C).

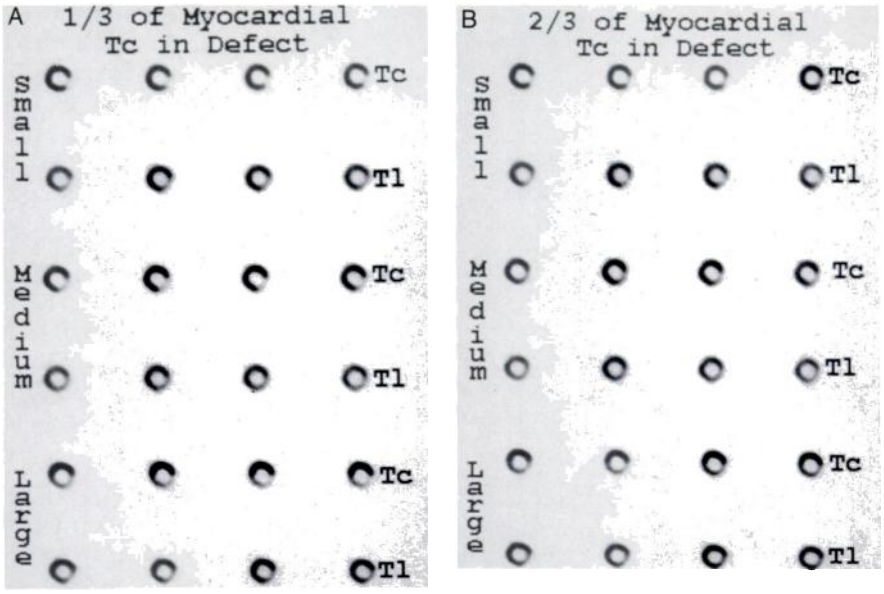

FIGURE 5. Defect sizes with 1/3 (A) and 2/3 (B) of the myocardial ^{99m}Tc in the defects. All had attenuating media present.

appeared to have subtle filling in of the rest image defect (Fig. 8), making it appear slightly smaller than the exercise defect. This may represent ^{99m}Tc downscatter into the ^{201}Tl window that was accentuated by background activity.

The myocardial-to-defect ^{201}Tl count ratio in phantom B's representation of infarct was 1.77, whereas phantom A's ratio in the representation of infarct (medium defect with attenuation media) was 2.96 (Table 1). This difference

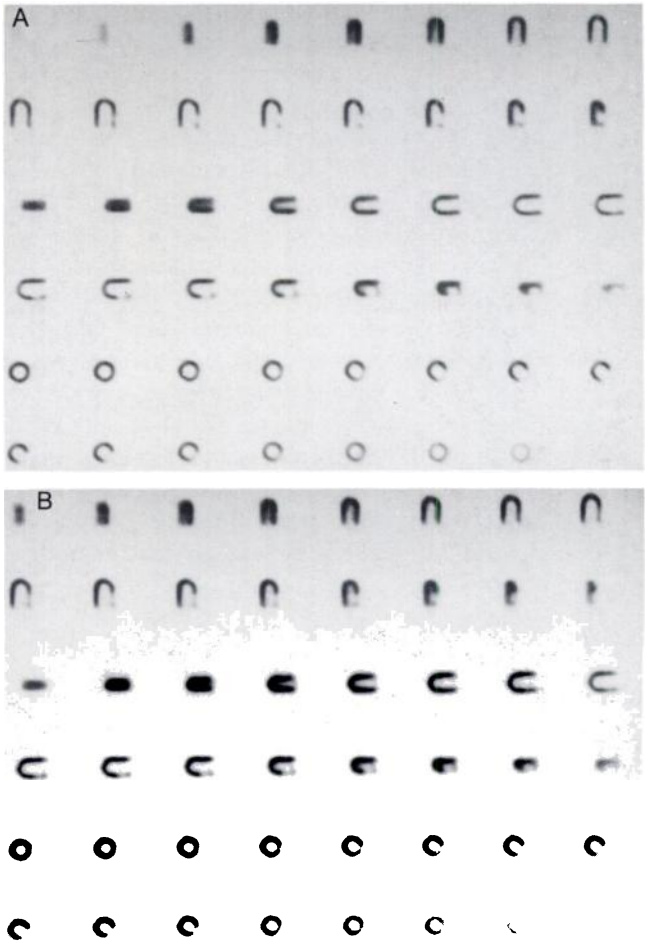

FIGURE 6. Simulated viable myocardium with ^{99m}Tc (A) and ^{201}Tl (B) images. Attenuating media present.

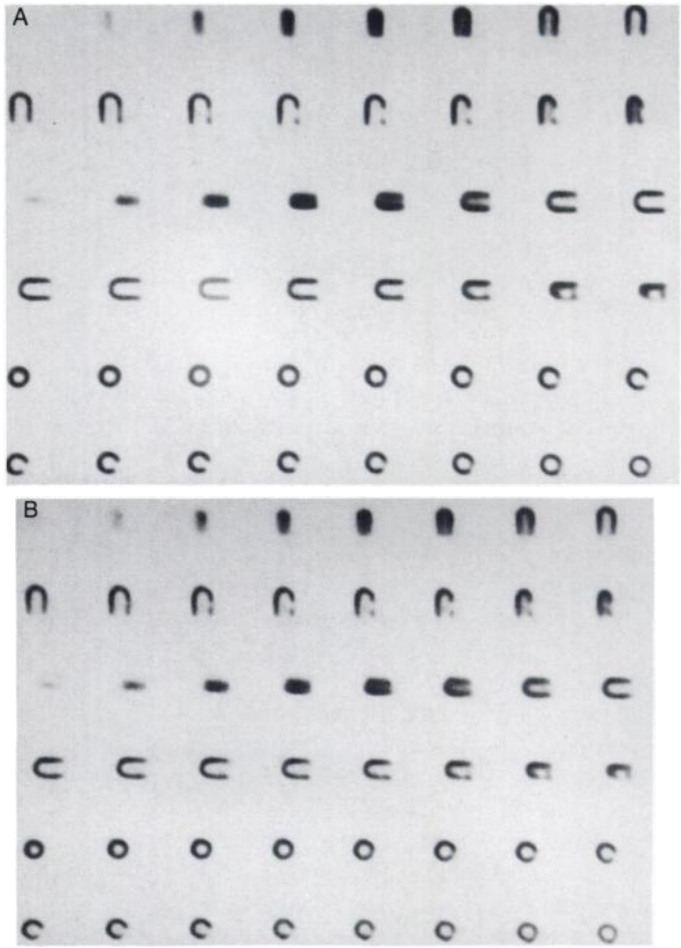

FIGURE 7. Simulated infarcted myocardium with ^{99m}Tc (A) and ^{201}Tl (B) images. Attenuating media present.

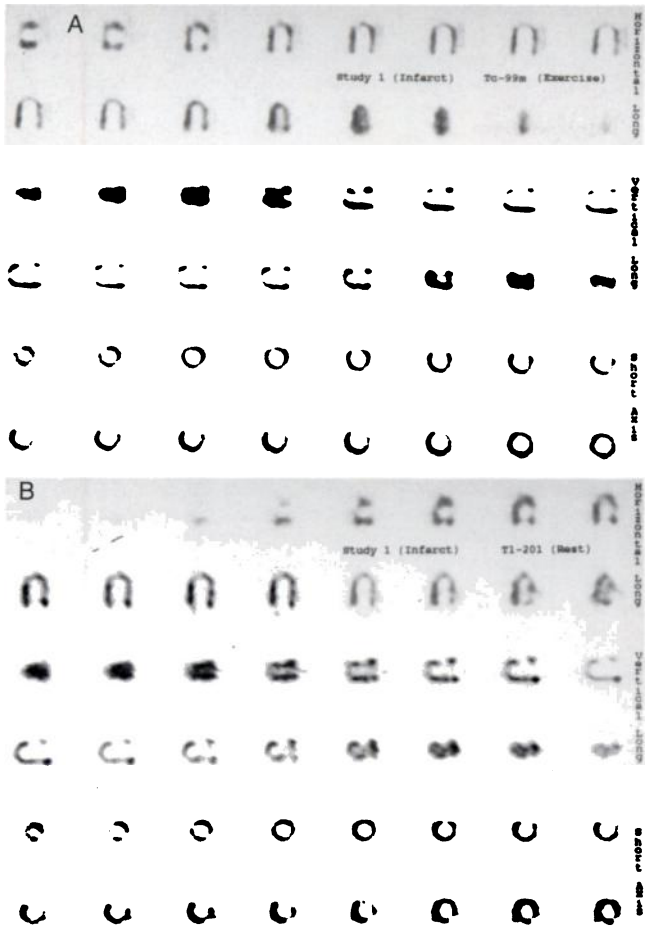

FIGURE 8. Simulated infarcted myocardium with ^{99m}Tc (A) and ^{201}Tl (B) images in the presence of background activity and attenuating media in phantom B.

A's ratio in the representation of infarct (medium defect with attenuation media) was 2.96 (Table 1). This difference occurred even though the myocardial decay-corrected activity concentrations in both studies were almost the same (1.6 and 1.7 μCi/ml in phantoms A and B respectively given that the activity concentration in phantom A had been tripled and acquisition time reduced accordingly). Restoration or energy-dependent filters could possibly be developed to minimize the effect of downscatter of ^{99m}Tc photons into the ^{201}Tl window. However, the development and evaluation of these approaches is beyond the scope of the present study.

Filling in of the rest defect was not visually apparent in phantom A's representation of infarct when no background activity was present (Fig. 7). The defect sizes measured using ^{201}Tl alone (single-agent studies) were minimally larger than those using ^{99m}Tc alone. The defect sizes measured by ^{201}Tl were smaller than those measured by ^{99m}Tc in the dual studies. However, the differences were not statistically significant and were similar in magnitude to the variation seen in the size determination method. Small differences in defect size as well as any ^{99m}Tc downscatter into the ^{201}Tl window potentially could cause the appearance of filling in of an infarct. However, the infarcts were correctly identified (6/6) by the observers when presented in short-axis, horizontal long-axis and vertical long-axis views. Therefore, subtle filling in of the rest image defects was below the clinical threshold of the observers for the identification of ischemia and is consistent with clinical observations (*24*).

The differences in tissue accumulation of the two isotopes in the peri-infarct or peri-ischemic regions may alter the size representations of the isotopes in patient studies. If ^{201}Tl is more likely to accumulate in peri-infarct myocardium, ^{201}Tl image defects may appear smaller than ^{99m}Tc defects. In clinical studies, it has been reported that ^{99m}Tc-sestamibi underestimates the size of the defect in patients with ischemia as compared to ^{201}Tl, but the correlation is weak and occasionally defects were larger using sestamibi (*17*). Documenting the correct size of the ischemic region would be needed. Further work may be needed to compare the defect sizes seen clinically with dual-isotope studies when compared to single-agent defect sizes.

Myocardial viability could also be assessed using the dual-isotope technique and late redistribution imaging to evaluate regions that appear infarcted on immediate images should be possible (*29*). In this study, we have shown that defect activity levels of ^{201}Tl less than myocardial levels produced myocardial-to-defect count ratios lower than those of infarcted defects and were qualitatively identifiable as ischemia rather than infarct (Fig. 6). Imaging at 24 hr if needed should not be problematic because counts from ^{201}Tl should be roughly 12-fold greater than those from ^{99m}Tc, and any contribution from ^{99m}Tc would be extremely small. Furthermore, rest-injection of thallium, as it is performed in the dual-isotope technique, may have a greater likelihood of demonstrating viable tissue when imaged within the first 2 hr after injection than would thallium that is injected during peak exercise and when no reinjection is performed.

Defect activity concentrations of ^{99m}Tc that were one-third and two-thirds of the normal myocardial activity were correctly identified in most cases (11/12) (Fig. 5). The one study that did not have a uniform interpretation was a study with two-thirds of the myocardial ^{99m}Tc activity in the defect (attenuating media present). These two protocols were chosen in an attempt to mimic different levels of myocardial wall involvement with ischemia or different levels of obstruction to perfusion in clinical settings. The defects were visually more subtle, and dramatic reductions in defect size measurements were identified.

CONCLUSIONS

Myocardial perfusion studies using simultaneously acquired dual-isotope rest ^{201}Tl/stress ^{99m}Tc-sestamibi images could save considerable patient study time and decrease the risk of artifacts due to patient motion or misalignment. We have shown that phantom images generated by the dual-isotope technique produce similar myocardium-to-defect count ratios and defect sizes to those produced using single-isotope techniques. Defects representing infarct, viable myocardium, minimal ischemia, moderate ischemia and severe

appropriate background activity and attenuating media to mimic clinical situations, defects representing infarct and ischemia can also be identified.

ACKNOWLEDGMENTS

This research was supported in part by Public Health Service grant S10-RR04176; NIH grants HL-17670 and CA33541 and Department of Energy grants DE-FG05-92ER60894 and DE-FG05-90ER75577.

REFERENCES

1. Ritchie JL, Zaret BL, Strauss HW, et al. Myocardial imaging with thallium-201: a multicenter study in patients with angina pectoris or acute myocardial infarction. *Am J Cardiol* 1978;42:345–350.
2. Ritchie JL, Trobaugh GB, Hamilton GW, et al. Myocardial imaging with thallium-201 at rest and during exercise. Comparison with coronary arteriography and resting and stress electrocardiography. *Circulation* 1977;56: 66–71.
3. Pantaleo N, Berman DS, Freeman M, Maddahi J, Swan HJ. Thallium myocardial scintigraphy and its use in the assessment of coronary artery disease. *Heart Lung* 1981;10:61–71.
4. Holman BL, Sporn V, Jones AG, et al. Myocardial imaging with technetium-99m-CPI: initial experience in the human. *J Nucl Med* 1987;28:13–18.
5. Wackers FJ, Berman DS, Maddahi J, et al. Technetium-99m-hexakis 2-methoxyisobutyl isonitrile: human biodistribution, dosimetry, safety, and preliminary comparison to thallium-201 for myocardial perfusion imaging. *J Nucl Med* 1989;30:301–311.
6. Dilsizian V, Rocco TP, Freedman NM, Leon MB, Bonow RO. Enhanced detection of ischemic but viable myocardium by the reinjection of thallium after stress-redistribution imaging. *N Engl J Med* 1990;323:141–146.
7. Hamilton GW, Trobaugh GB, Ritchie JL, Williams DL, Weaver WD, Gould KL. Myocardial imaging with intravenously injected thallium-201 in patients with suspected coronary artery disease: analysis of technique and correlation with electrocardiographic, coronary anatomic and ventriculographic findings. *Am J Cardiol* 1977;39:347–354.
8. Kiat H, Van Train K, Maddahi J, et al. Development and prospective application the diagnosis of coronary artery disease. *Am Heart J* 1990;120: 1255–1266.
9. Borges-Neto S, Coleman RE, Jones RH. Perfusion and function at rest and treadmill exercise using technetium-99m-sestamibi: comparison of one and two-day protocols in normal volunteers. *J Nucl Med* 1990;31:1128–1132.
10. Maddahi J, Kiat H, Van Train K, et al. Myocardial perfusion imaging with technetium-99m sestamibi SPECT in the evaluation of coronary artery disease. *Am J Cardiol* 1990;66:55E–62E.
11. Heo J, Kegel J, Iskandrian AS, Cave V, Iskandrian BB. Comparison of same-day protocols using technetium-99m-sestamibi myocardial imaging. *J Nucl Med* 1992;33:186–191.
12. Sochor H. Technetium-99m sestamibi in chronic coronary artery disease: the European experience. *Am J Cardiol* 1990;66:91E–96E.
13. Berman DS, Kiat H, Maddahi J. The new ^{99m}Tc myocardial perfusion imaging agents: ^{99m}Tc-sestamibi and ^{99m}Tc-teboroxime. *Circulation* 1991; 84:17–21.
14. Kiat H, Maddahi J, Roy LT, et al. Comparison of technetium-99m methoxy isobutyl isonitrile and thallium-201 for evaluation of coronary artery disease by planar and tomographic methods. *Am Heart J* 1989;117:1–11.
15. Maisey MN, Lowry A, Bischof DA, et al. European multi-centre comparison of thallium-201 and technetium-99m methoxyisobutylisonitrile in ischaemic heart disease. *Eur J Nucl Med* 1990;16:869–872.
16. Berman DS, Kiat H, Van Train K, Garcia E, Friedman J, Maddahi J. Technetium-99m-sestamibi in the assessment of chronic coronary artery disease. *Semin Nucl Med* 1991;21:190–212.
17. Maublant JC, Marcaggi X, Lusson JR, et al. Comparison between thallium-201 and technetium-99m methoxyisobutyl isonitrile defect size in single-photon emission computed tomography at rest, exercise and redistribution in coronary artery disease. *Am J Cardiol* 1992;69:183–187.
18. Narahara KA, Villanueva MJ, Thompson CJ, Brizendine M, Mena I. Comparison of thallium-201 and technetium-99m hexakis 2-methoxyisobutyl isonitrile single-photon emission computed tomography for estimating the extent of myocardial ischemia and infarction in coronary artery disease. *Am J Cardiol* 1990;66:1438–1444.
19. Canby RC, Silber S, Pohost GM. Relations of the myocardial imaging agents ^{99m}Tc-MIBI and ^{201}Tl to myocardial blood flow in a canine model of myocardial ischemic insult. *Circulation* 1990;81:289–296.
20. Tartagni F, Dondi M, Limonetti P, et al. Dipyridamole technetium-99m-2-methoxyisobutylisonitrile tomoscintigraphic imaging for identifying diseased coronary vessels: comparison with thallium-201 stress-rest study. *J Nucl Med* 1991;32:369–376.
21. Beller GA, Watson DD. Physiological basis of myocardial perfusion imaging with the technetium-99m agents [see comments]. *Semin Nucl Med* 1991;21: 173–181.
22. Najm YC, Maisey MN, Clarke SM, Fogelman I, Curry PV, Sowton E. Exercise myocardial perfusion scintigraphy with technetium-99m methoxyisobutylisonitrile: a comparative study with thallium-201. *Int J Cardiol* 1990;26:93–102.
23. Iskandrian AS, Heo J, Kong B, Lyons E, Marsch S. Use of technetium-99m isonitrile (RP-30A) in assessing left ventricular perfusion and function at rest and during exercise in coronary artery disease, and comparison with coronary arteriography and exercise thallium-201 SPECT imaging. *Am J Cardiol* 1989;64:270–275.
24. Kiat H, Friedman J, Van Train K, Wang FP. Simultaneous rest Tl-201/ stress Tc-99m sestamibi dual isotope myocardial perfusion SPECT: a pilot study [Abstract]. *J Nucl Med* 1991;32:1006.
25. Berman D, Friedman J, Kiat H, Wang FP, Bietendorf J, Van Train K. Accuracy of separate acquisition dual isotope myocardial perfusion SPECT: results of a large clinical trial [Abstract]. *J Am Coll Cardiol* 1992;19:202A.
26. Matzer L, Kiat H, Friedman J, et al. Separate acquisition dual isotope myocardial perfusion SPECT using pharmacologic stress [Abstract]. *J Am Coll Cardiol* 1992;19:127A.
27. Atkins HL, Budinger TF, Lebowitz E, et al. Thallium-201 for medical use. Part 3: human distribution and physical imaging properties. *J Nucl Med* 1977;18:133–140.
28. Normand B, Maublant J, d'Agrosa MC, Lusson JR, Cassagnes J, Veyre A. Comparison of the myocardial distributions of ^{201}Tl and ^{99m}Tc-MIBI on SPECT images. *Nucl Med Commun* 1991;12:393–396.
29. Kiat H, Berman DS, Maddahi J, et al. Late reversibility of tomographic myocardial thallium-201 defects: an accurate marker of myocardial viability. *J Am Coll Cardiol* 1988;12:1456–1463.

EDITORIAL

Simultaneous Thallium-201/Technetium-99m Dual-Isotope Cardiac SPECT: Ready for Prime Time?

Simultaneous dual-isotope SPECT myocardial perfusion imaging with ^{201}Tl and ^{99m}Tc-sestamibi may potentially provide a very attractive means to evaluate patients with known or suspected coronary artery disease. A ^{201}Tl dose is administered with the patient at rest, and a ^{99m}Tc-sestamibi dose is then given during peak exercise. Subsequent dual-isotope imaging could simultaneously provide images of both rest and stress perfusion distribution. Potential clinical advantages of this approach are substantial and multifold. Since only one single SPECT acquisition is required, patient throughput could be doubled, substantially increasing the cost-effectiveness of instrumentation and personnel and increasing the satis-

Received Aug. 4, 1993; revision accepted Aug. 4, 1993.

For correspondence or reprints contact: E. Gordon DePuey, MD, Division of Nuclear Medicine, St. Lukes–Roosevelt Hospital Center, Amsterdam Ave. at 114th St., New York, NY 10025.